A Descrição dos dados

Figure 4: Geographical Distribution of Main Variables

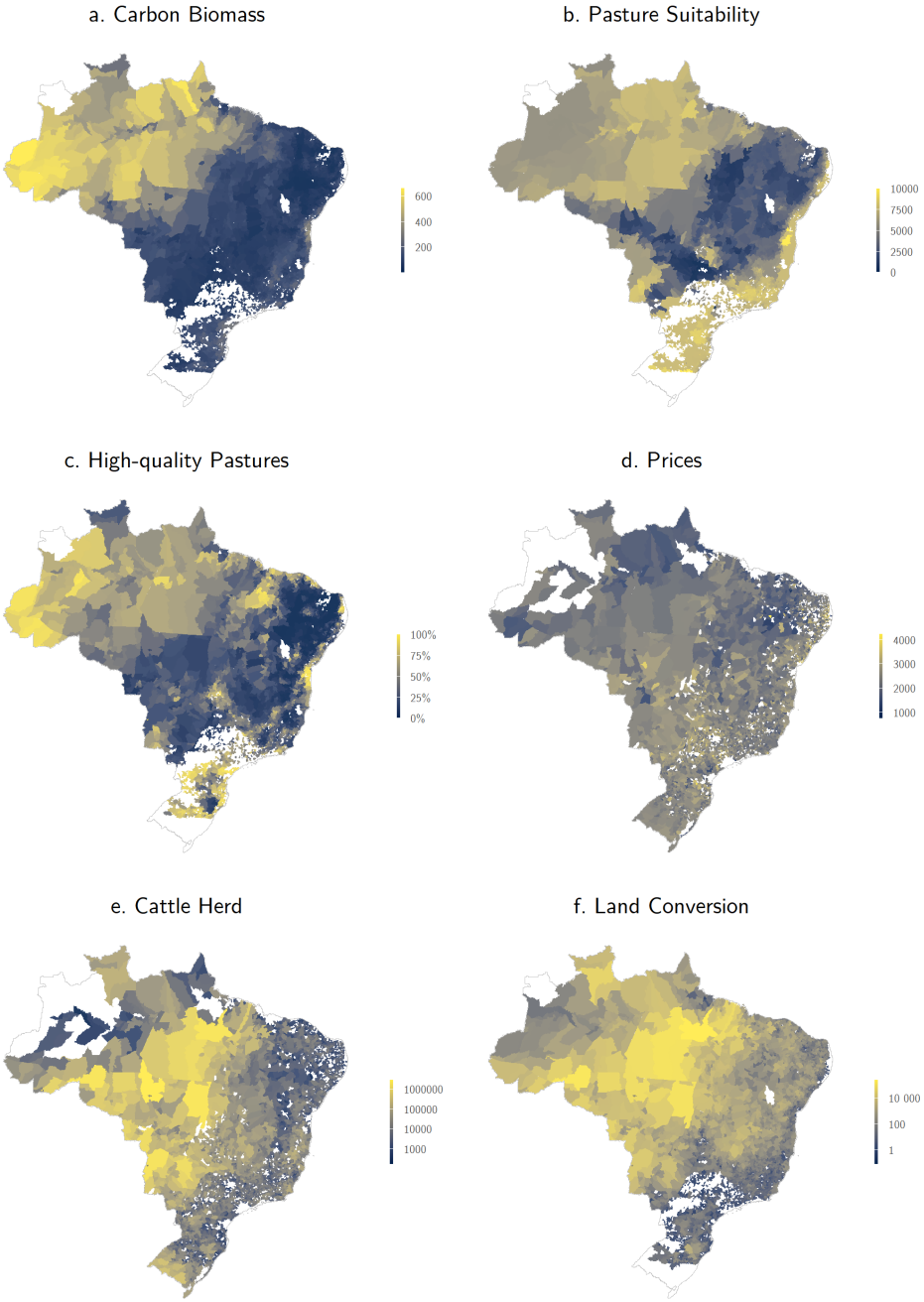

This figure plots for each municipality in sample, **(a)** the carbon biomass density, measured in tons of CO_2 per hectare; **(b)** the index of pasture suitability from FAO-GAEZ; **(c)** the share of pastures with high quality, in 2017; **(d)** the average per capita price of cattle sold for slaughter in 2017, measured in R$ of 2022; **(e)** the herd of cattle at the end of 2017; **(f)** total area converted from natural vegetation to pasture in 2006 and 2007, measured in hectares.

A.1 Municipalities

The number and area of municipalities – the smallest administrative divisions in Brazil – change over time due to the creation of new municipalities or the annexation of existing ones. To address this issue, I use the concept of *minimum comparable areas* (AMCs), which are time-consistent regions enabling the construction of municipality panel data. I follow the methodology of Ehrl (2017), who developed AMCs for the period 1872–2010, and extend it to account for municipal boundary changes between 2010 and 2022.

All official statistics at the municipality level are aggregated to the AMC level. Additionally, I calculate the predominant biome in each AMC, defined as the biome occupying the largest share of its area, based on the methodology from IBGE (2024). Hereafter, I refer to these minimum comparable areas simply as municipalities.

A.2 Cattle herd

I use two data sources to estimate the herd of cattle per municipality per year. The primary source is the *Agricultural Census* from the Brazilian Institute of Geography and Statistics (IBGE) for the years 1995, 2006, and 2017. The census collects detailed data on agricultural establishments and their activities, with each production unit serving as the observation unit. The second source is the annual livestock production surveys (*Pesquisa da Pecuária Municipal*, from IBGE). This dataset is primarily derived from administrative records of the Foot-and-Mouth Disease Vaccination Campaigns[8], compiled by state and local inspectorates as well as veterinary posts.

To approximate h_{mt}, which is a theoretical measure of livestock per plot of land, I normalize the municipality's head of cattle by its total area. This normalization ensures a temporally and spatially consistent measure of livestock density across municipalities of varying sizes. It then facilitates cross-sectional and temporal comparisons, as it accounts for differences in land availability that could otherwise confound the relationship between herd size and other variables of interest.

A.3 Cattle prices

I derive local cattle prices from sales and revenue data obtained in the 2006 and 2017 administrations of *Agricultural Census*. These represent the cattle price per animal sold for slaughter in each municipality. To project prices for the subsequent year, I adjust them using variations in a national cattle price index. This variation is computed by comparing the average index in the census year with the average for the 12 months following the census.

The cattle price index, sourced from the *Center for Advanced Studies in Applied Economics* (CEPEA), measures the average price of 15 kg of carcass weight at slaughter for finished bull sales in São Paulo State. São Paulo prices are industry benchmarks; less productive regions

[8] *Campanha de Vacinação contra a Febre Aftosa*

typically have lower prices but exhibit similar trends. All prices are deflated to December 2022 values using the Extended National Consumer Price Index (IPCA).

A.4 Land use

Land-use data is sourced from the *MapBiomas Project* (Souza et al. 2020), which provides annual 30-meter resolution maps derived from Landsat imagery. Using a random forest classifier, spatial-temporal filters to minimize noise, and thorough accuracy assessments, MapBiomas classifies each pixel into predefined land-use categories. Year-on-year transition matrices are created by comparing pixel classifications between consecutive years, enabling detailed tracking of land-use changes over time.

I aggregate land-use statistics and transitions into four categories: agriculture, pasture, natural vegetation, and other (e.g., non-classified pixels, urban areas, and water). My analysis focuses on transitions from natural vegetation to pasture. The conditional choice probabilities ρ_{mt} are estimated non-parametrically as the share of natural vegetation pixels converted to pasture in each municipality for each pair of successive years.

A.5 Pasture quality

For this study, I use high-resolution data on the quality of Brazilian pastures developed as part of the *MapBiomas Project* (Santos et al. 2022). This dataset is constructed based on the Normalized Difference Vegetation Index (NDVI), a widely used metric for assessing vegetation health and productivity. The NDVI is derived by comparing the reflectance of electromagnetic radiation in the red and near-infrared portions of the spectrum, utilising imagery from Landsat satellites. It serves as an effective proxy for vegetative vigour, with higher values generally indicating healthier, more productive vegetation.

Pasture quality is inherently influenced by local environmental conditions, meaning that a pasture considered degraded in one biome might still perform adequately in another (Dias-Filho 2014). To account for this geographical heterogeneity, the dataset normalizes the median NDVI values using biome-specific maximum and minimum percentiles. This normalization ensures that comparisons are made relative to the optimal vegetation conditions within each biome. After normalization, the NDVI values are categorised into three classes of vegetative vigour, corresponding to the states of high, medium and low vigour.

The use of NDVI as an indicator of pasture quality is grounded in its ability to reflect biological degradation by capturing the health of vegetation and its forage productivity. However, this measure is less effective at detecting agricultural degradation, which involves increased weed presence that competes pastures out (Lapig et al. 2023). As such, while the data is highly suited to assessing the biological quality of pastures, it may underestimate the full extent of degradation in areas where agricultural degradation is more prevalent.

By employing this dataset, my analysis focuses on the counterfactual scenarios of improving the *biological* quality of pastures. For a broader discussion on the distinctions between

biological and agricultural degradation, as well as the causes and consequences of pasture degradation, see Appendix B.

To construct an indicator of pasture quality for each municipality, I calculate the share of its pasture area classified with high vegetative vigour. This approach offers the advantage of producing a continuous variable, which provides greater granularity in capturing variations in pasture quality across municipalities and over time. By focusing on the share of high-vigour pastures, the measure inherently accounts for the quality of all remaining pasture areas, implicitly classifying those with lower vigour as degraded. This includes areas identified as either mildly or severely degraded based on their vegetative state.

This indicator offers a more flexible metric for evaluating policy changes in pasture quality and their potential impacts compared to a categorical variable. In counterfactual scenarios, it enables the assessment of gradual increases in the share of high-quality pastures. These improvements represent a hypothetical recovery or restoration of degraded pasture areas, encompassing the entire spectrum of degradation, from mild to severe.

A.6 International trade

To address endogeneity concerns in price determination, I use exogenous demand shocks derived from trends in Chinese agricultural imports as instrumental variables. These shocks represent external demand variations that are independent of local supply conditions. Specifically, I construct a shift-share instrumental variable that allocates aggregate demand shocks from China to Brazilian municipalities in proportion to their respective market shares. This approach allows me to isolate exogenous variation in local prices that stems from global market conditions.

The trade data for constructing this instrument come from the *CEPII BACI - International Trade Database at the Product-Level* (Gaulier et al. 2010). The BACI dataset provides detailed bilateral trade flows between more than 200 countries and covers approximately 5,000 products classified using the Harmonized System (6-digit codes). The dataset spans the period 1995 – 2022, and I align my analysis with the broader China-shock literature by using 2000 as the base year, reflecting China's accession to the World Trade Organization (WTO) in 2001.

A.7 Aboveground carbon biomass

In the model, the returns to maintaining fields as natural vegetation depend on their aboveground carbon biomass. For this, I rely on high-resolution (30-meter) spatial data of Aboveground Live Woody Biomass (AGB), measured in megagrams per hectare for the year 2000. This data was developed by Harris et al. (2021), based on the methodology developed by Baccini et al. (2012). The authors integrate ground-based biomass measurements from over 700,000 sample locations with satellite imagery from Landsat, processed through a machine-learning predictive model.

Finally, I convert the biomass weight provided in the dataset to the potential of CO2 release, accounting for the molecular weight of carbon dioxide, following Araujo, Costa, et al. (2020). To

convert aboveground biomass to potential CO2 release, I first divide the weight by 2 to estimate the carbon content, as biomass is roughly 50% carbon. Then, I multiply this carbon content by the ratio of the molecular weights of CO2 (44) to carbon (12), which converts the carbon content into the equivalent amount of carbon dioxide. This conversion enables direct comparison with international estimations of the social cost of carbon.

A.8 Weather controls

For weather controls, I utilize data from the *TerraClimate* dataset, which offers global high-resolution monthly climate and water balance data (Abatzoglou et al. 2018). TerraClimate integrates climatological normals with time-varying data to produce comprehensive monthly estimates. I include data on minimum, mean, and maximum temperatures, as well as the Palmer Drought Severity Index (PDSI), a standardized measure of long-term moisture availability that accounts for precipitation, evapotranspiration, and soil water balance. The PDSI is particularly relevant for its impact on pasture quality, as it reflects the availability of water for plant growth, with drought conditions leading to reduced forage productivity and quality.

A.9 Transportation cost and market access

To control for the effects of transportation infrastructure on deforestation, I use quality-adjusted transportation cost estimates and a measure of market access to other regions (Araujo, Assunção, et al. 2023; Araujo, Costa, et al. 2024). These metrics are based on detailed geographical data on roads, waterways, railways, and ports. They estimate the cost of transporting goods to international markets and quantify a municipality's connectivity to other regions. The market access measure is derived from an inter-regional trade model that incorporates population distribution and trade elasticity.

A.10 Pasture suitability

To account for biophysical factors influencing agricultural productivity, I use a pasture suitability index developed by the *Food and Agriculture Organization's (FAO) Global Agro-Ecological Zones project* (Velthuizen et al. 2007). This index integrates multiple dimensions of climate, soil, and terrain characteristics to estimate attainable productivity for pasture, providing a score from 0 to 10000. The climate factors include thermal conditions, the length of the growing period, climate variability, and limitations such as cold temperatures or insufficient moisture. Soil characteristics, such as depth, type, and quality, are also considered, along with terrain features like slope. With it, I can control for several environmental determinants of pasture productivity at once.

B Details on pasture degradation

Pasture degradation refers to the decline in a pasture's capacity to support livestock. This phenomenon is characterised by a progressive loss of pasture vigour and resilience, impairing its ability to recover after grazing or adverse environmental conditions. As a result, pasture degradation poses a significant challenge to the sustainability of livestock production systems. Pasture degradation can be broadly categorised into two main types: agricultural degradation and biological degradation (Dias-Filho 2014).

Agricultural degradation is primarily associated with the encroachment of invasive plant species and the proliferation of weeds. These competing plants reduce the availability of high-quality forage for livestock, making grazing increasingly inefficient. Over time, the dominance of weeds further suppresses pasture productivity, creating a feedback loop of reduced forage availability, decreased livestock performance, and declining agricultural output.

Biological degradation, in contrast, arises from soil deterioration. It manifests as a reduction in vegetation cover, leading to soil erosion, loss of organic matter, and the depletion of critical nutrients needed to sustain plant growth. This form of degradation is more severe than agricultural degradation because it undermines the fundamental capacity of the soil to support any vegetation, further exacerbating environmental and productivity challenges.

The drivers of degradation include a combination of improper grazing practices and external environmental factors. Inadequate grazing management – such as overgrazing, poor rest period planning, neglect of soil fertility restoration, and excessive reliance on fire – contributes significantly to both agricultural and biological degradation. Additionally, factors like pest infestations, plant diseases, and adverse environmental conditions (e.g., low rainfall or poor soil fertility) amplify the degradation process.

Recovery efforts typically involve interventions such as soil fertility restoration, reseeding with high-quality forage species, and implementing rotational grazing systems. These measures not only address the symptoms of degradation but also tackle its root causes, including improper grazing management and nutrient imbalances (Dias-Filho 2015).

In Brazil, pasture degradation remains a pervasive issue, affecting both the environmental health of grazing lands and the economic viability of livestock farming. Although recent improvements have been documented, degraded pastures still constitute a substantial share of total pastureland. For instance, in 2018, 58.9% of pastures in Brazil exhibited some level of degradation (Santos et al. 2022).

The recovery of degraded pastures is often presented in the literature as a key component of agricultural intensification strategies, with the potential to enhance productivity while reducing pressure on natural ecosystems. By improving the productive capacity of existing pastures, some argue that pasture recovery could discourage the need for additional land conversion and thus help curb deforestation (Carlos et al. 2022; Dias-Filho 2012; Feltran-Barbieri et al. 2021).

However, while this premise is widely cited, it remains largely untested in the context of comprehensive economic models of land use. As demonstrated in this paper, the interplay be-

tween pasture quality and land conversion is complex. While higher-quality pastures can indeed reduce deforestation through increased conversion costs (the Borlaug effect), the associated productivity gains may simultaneously incentivise land conversion by raising the economic returns to grazing (the Jevons effect). These countervailing forces suggest that the potential of pasture recovery as a deforestation mitigation strategy must be carefully scrutinised, particularly in policy discussions aimed at achieving sustainable agricultural development.

C Demonstrations

C.1 Intensive Margin

C.1.1 Derivation of the optimality condition

The first order condition states that, at the optimum, marginal revenue equals the discounted future marginal value of the herd.

$$\begin{aligned}\frac{\partial r(c_{it};\boldsymbol{s_{mt}})}{\partial c_{it}} &= -\beta\,\mathbb{E}_t\left[\frac{\partial \mathcal{V}(h_{it+1};\boldsymbol{s_{mt+1}})}{\partial h_{it+1}}\frac{\partial h_{it+1}}{\partial c_{it}}\right] \\ &= \beta\,\mathbb{E}_t\left[\frac{\partial \mathcal{V}(h_{it+1};\cdot)}{\partial h_{it+1}}\right]\end{aligned} \tag{9}$$

And by the envelope theorem, at the optimum, the marginal value equals the discounted future marginal value, increased by ϕ, minus marginal costs.

$$\begin{aligned}\frac{\partial \mathcal{V}(h_{it};\boldsymbol{s_{mt}})}{\partial h_{it}} &= -\frac{\partial \psi(h_{it};\boldsymbol{s_{mt}})}{\partial h_{it}} + \beta\,\mathbb{E}_t\left[\frac{\partial \mathcal{V}(h_{it+1};\boldsymbol{s_{mt+1}})}{\partial h_{it+1}}\frac{\partial h_{it+1}}{\partial h_{it}}\right] \\ &= -\frac{\partial \psi(h_{it};\cdot)}{\partial h_{it}} + \beta(1+\phi)\,\mathbb{E}_t\left[\frac{\partial \mathcal{V}(h_{it+1};\cdot)}{\partial h_{it+1}}\right]\end{aligned} \tag{10}$$

Substituting 9 in 10 yields:

$$\frac{\partial \mathcal{V}(h_{it};\cdot)}{\partial h_{it}} = -\frac{\partial \psi(h_{it};\cdot)}{\partial h_{it}} + (1+\phi)\frac{\partial r(c_{it};\cdot)}{\partial c_{it}}$$

Forwarding it one period, and substituting back into 9, we reach the optimality condition of the problem, given by the following Euler equation:

$$\frac{\partial r(c_{it};\cdot)}{\partial c_{it}} = \beta\,\mathbb{E}_t\left[(1+\phi)\frac{\partial r(c_{it+1};\cdot)}{\partial c_{it+1}} - \frac{\partial \psi(h_{it+1};\cdot)}{\partial h_{it+1}}\right] \tag{11}$$

That means optimal slaughter c_{it} is that which equates marginal revenue from a sale at t to the discounted expected marginal opportunity cost of the forgone sale at $t+1$. Each new animal sold increases revenues at t, but reduces the herd for the next period, reducing potential revenues but also reducing the herd carrying cost.

Note that for every plot i in municipality m, the farmers face the same optimality condition. Therefore, I can denote the optimal choice $h_{it}^{\star}$ for every plot in municipality m as simply h_{mt}. From the specified functional forms, marginal revenues and costs are given by:

$$\frac{\partial r(c_{it};\cdot)}{\partial c_{it}} = \alpha_p p_{mt}$$

$$\frac{\partial r(c_{it+1};\cdot)}{\partial c_{it+1}} = \alpha_p p_{mt+1}$$

$$\frac{\partial \psi(h_{mt+1};\cdot)}{\partial h_{mt+1}} = \delta h_{mt+1} + \boldsymbol{x_{it+1}}\gamma_x + \gamma_g + \gamma_t(t+1) + \varepsilon_{it+1}$$

With this, I can write the Euler equation 11 as follows.

$$\frac{1}{\beta}\alpha_p p_{mt} = \alpha_p(1+\phi)\,\mathbb{E}_t[p_{mt+1}] - \mathbb{E}_t\Big[\delta h_{mt+1} + \boldsymbol{x_{it+1}}\gamma_x + \gamma_g + \gamma_t(t+1) + \varepsilon_{it+1}\Big] \tag{12}$$

Note that, from the law of motion, the process of deciding on c_{it} at period t also defines h_{mt+1}. Hence, I can write $\mathbb{E}_t[h_{mt+1}] = h_{mt+1}$.

$$\delta h_{mt+1} = \alpha_p(1+\phi)\,\mathbb{E}_t[p_{mt+1}] - \frac{1}{\beta}\alpha_p p_{mt} - \mathbb{E}_t[\boldsymbol{x_{it+1}}\gamma_x] - +\gamma_g - \gamma_t(t+1) - \mathbb{E}_t[\varepsilon_{it+1}]$$

Which can be then rewritten as 2.

C.2 Extensive Margin

C.2.1 Derivation of the optimality condition

I further define the ex-ante value function, which is the expected value of being in state $\boldsymbol{s_{mt}}$ before the realization of shocks $\boldsymbol{\nu_{it}}$.

$$\overline{V}(0,\, \boldsymbol{s_{mt}}) \equiv \mathbb{E}_{\boldsymbol{\nu}}\Big[\, V(0,\, \boldsymbol{s_{mt}}, \boldsymbol{\nu_{it}})\,\Big]$$

And the conditional value functions, which are the present value of choosing j in period t and behaving optimally afterwards. Here, consider $\pi_{mt}(j)$ to mean the payoffs $\pi(j, \boldsymbol{s_{mt}}, \boldsymbol{\nu_{it}})$ net of the idiosyncratic shocks ν_{ijt}.

$$v(0, \boldsymbol{s_{mt}}) = \pi_{mt}(0) + \beta\,\mathbb{E}\Big[\,\overline{V}(0,\, \boldsymbol{s_{mt+1}}) \mid \boldsymbol{s_{mt}}\,\Big] \tag{13}$$

$$v(1, \boldsymbol{s_{mt}}) = \pi_{mt}(1) \tag{14}$$

Assumption 4 of EV1 extensive margin shocks implies the conditional choice probabilities have closed-form logit solutions. That is to say, the probability of observing a choice of land

conversion from forest to pastures ($j_t = 1$), is given by:

$$\rho(1 \mid \boldsymbol{s_{mt}}) = \frac{\exp\Big[\, v(1, \boldsymbol{s_{mt}}) \,\Big]}{\exp\Big[\, v(0, \boldsymbol{s_{mt}}) \,\Big] + \exp\Big[\, v(1, \boldsymbol{s_{mt}}) \,\Big]}$$

To lighten notation, I denote henceforth $\rho(1 \mid \boldsymbol{s_{mt}}) = \rho_{mt}$ and $\rho(0 \mid \boldsymbol{s_{mt}}) = 1 - \rho_{mt}$, which follows from the binary choice set. Using the Hotz et al. (1993) inversion, I can rearrange the conditional choice probabilities and relate their ratio to the difference in conditional value functions:

$$\log\left(\frac{\rho_{mt}}{1-\rho_{mt}}\right) = v(1, \boldsymbol{s_{mt}}) - v(0, \boldsymbol{s_{mt}}) \tag{15}$$

And applying Arcidiacono and Miller (2011)'s *Lemma 1* to the EV1 case, the ex-ante value function can be rewritten with respect to the conditional value function of any arbitrary choice:

$$\bar{V}_{it}(0) = v(1, \boldsymbol{s_{mt}}) - \log(\rho_{mt}) + \gamma \tag{16}$$

Where γ is the Euler-Mascheroni constant. In equation 15, I substitute the conditional value functions with 13 and 14, and apply equation 16 forwarded one period:

$$\begin{aligned}
\log\left(\frac{\rho_{mt}}{1-\rho_{mt}}\right) &= \pi_{mt}(1) - \pi_{mt}(0) - \beta\, \mathbb{E}_t\Big[\, \bar{V}_{it+1}(0) \Big] \\
&= \pi_{mt}(1) - \pi_{mt}(0) - \beta\, \mathbb{E}_t\Big[\, \pi_{mt+1}(1) - \log(\rho_{mt+1}) + \gamma \Big]
\end{aligned}$$

Now, I open $\pi_{mt+1}(1)$ to include the intensive margin value function.

$$\begin{aligned}
\log\left(\frac{\rho_{mt}}{1-\rho_{mt}}\right) &= -\Psi(\boldsymbol{s_{mt}}) + \mathcal{V}(h_{mt} = 0, \boldsymbol{s_{mt}}) + \xi_{mt} - \pi_{mt}(0) \\
&- \beta\, \mathbb{E}_t\Big[-\Psi(\boldsymbol{s_{mt+1}}) + \mathcal{V}(h_{mt+1} = 0, \boldsymbol{s_{mt+1}}) + \xi_{mt+1} - \log(\rho_{mt+1}) + \gamma \Big]
\end{aligned} \tag{17}$$

Before advancing, I first develop the following difference of intensive-margin value functions. From now on, I denote optimal decisions in the path where the plot is deforested at t using one-asterisk-variables $(*)$, and where it was deforested at $t+1$ using two-asterisk-variables $(**)$.

$$\begin{aligned}
\mathcal{V}(h_{mt} = 0, \boldsymbol{s_{mt}}) &- \beta\, \mathbb{E}_t\Big[\, \mathcal{V}(h_{mt+1} = 0, \boldsymbol{s_{mt+1}}) \Big] \\
&= r(c^*_{it}; \cdot \mid h_{mt} = 0) + \beta\, \mathbb{E}_t\Big[\, \mathcal{V}(h^*_{mt+1}; \cdot) \Big] \\
&- \beta\, \mathbb{E}_t\Bigg[\, r(c^{**}_{it+1}; \cdot \mid h_{mt+1} = 0) + \beta\, \mathbb{E}_{t+1}\Big[\, \mathcal{V}(h^{**}_{mt+2}; \cdot) \Big] \Bigg]
\end{aligned}$$

And developing further:

$$\begin{aligned}\mathcal{V}(h_{mt}=0,\boldsymbol{s_{mt}}) - \beta\,\mathbb{E}_t\Big[\,\mathcal{V}(h_{mt+1}=0,\boldsymbol{s_{mt+1}})\Big] \\ = r(c^*_{it};\cdot \mid h_{mt+1}=0) + \beta\,\mathbb{E}_t\Big[\,r(c^*_{it+1};\cdot) - \psi(h^*_{mt+1};\cdot) + \beta\;\mathbb{E}_{t+1}[\mathcal{V}(h^*_{mt+2};\cdot)]\Big] \\ - \beta\,\mathbb{E}_t\Big[\,r(c^{**}_{it+1};\cdot \mid h_{mt+1}=0) + \beta\,\mathbb{E}_{t+1}\Big[\,\mathcal{V}(h^{**}_{mt+2};\cdot)\Big]\Big]\end{aligned}$$

The revenues $r(c^*_{it+1};\cdot)$ and $r(c^{**}_{it+1};\cdot \mid h_{mt+1}=0))$ are not equal, because the latter comes from the initial herd allocation at $t+1$. In these initial allocations, it can be shown using the law of motion that the consumptions alone define the herd that is left for the next period. That is:

$$\begin{aligned}c^*_{it\,|\,h_{mt}=0} &= -h^*_{mt+1} \\ c^{**}_{it+1\,|\,h_{mt+1}=0} &= -h^{**}_{mt+2}\end{aligned} \tag{18}$$

More importantly, it can be shown that $h^*_{mt+2} = h^{**}_{mt+2}$. It happens because the optimal choice of next-period herd follows from the intensive-margin Euler condition (equation 11) and is only forward-looking. Regardless of inherited herd, the rancher will consume optimally so that they end the period with the herd defined by the same optimality condition.

It means that, whether the rancher deforests at t or at $t+1$, at the end of $t+1$ they have herd size $h^*_{mt+2} = h^{**}_{mt+2}$. It follows then, that $\mathcal{V}(h^*_{mt+2};\cdot) = \mathcal{V}(h^{**}_{mt+2};\cdot)$. That is to say, the property of finite dependence holds and I can difference out the continuation values. Therefore, we can write the difference as:

$$\begin{aligned}\mathcal{V}(h_{mt}=0,\boldsymbol{s_{mt}}) - \beta\,\mathbb{E}_t\Big[\,\mathcal{V}(h_{mt+1}=0,\boldsymbol{s_{mt+1}})\Big] \\ = r(c^*_{it};\cdot \mid h_{mt}=0) + \beta\,\mathbb{E}_t\Big[\,r(c^*_{it+1};\cdot) - \psi(h^*_{mt+1};\cdot) - r(c^{**}_{it+1};\cdot \mid h_{mt+1}=0)\Big]\end{aligned}$$

Now we can return to the equation 17 and substitute this difference.

$$\begin{aligned}\log\left(\frac{\rho_{mt}}{1-\rho_{mt}}\right) = -\Psi(\boldsymbol{s_{mt}}) + \xi_{mt} - \pi_{mt}(0) - \beta\,\mathbb{E}_t\Big[-\Psi(\boldsymbol{s_{mt+1}}) + \xi_{mt+1} - \log(\rho_{mt+1}) + \gamma\Big] \\ + r(c^*_{it};\cdot \mid h_{mt}=0) + \beta\,\mathbb{E}_t\Big[\,r(c^*_{it+1};\cdot) - \psi(h^*_{mt+1};\cdot) - r(c^{**}_{it+1};\cdot \mid h_{mt+1}=0)\Big]\end{aligned}$$

Now, using the specified functional forms for intensive margin revenues and costs(1), extensive margin payoffs (**??**), and the results from 18.

$$\begin{aligned}\log\left(\frac{\rho_{mt}}{1-\rho_{mt}}\right) + \beta\gamma = -\Psi(\boldsymbol{s_{mt}}) + \xi_{mt} - \alpha_b b_m - \xi_{mt} \\ - \beta\,\mathbb{E}_t\Big[-\Psi(\boldsymbol{s_{mt+1}}) + \xi_{mt+1} - \log(\rho_{mt+1})\Big] \\ - \alpha_p p_{mt} h^*_{mt+1} + \beta\alpha_p\,\mathbb{E}_t\Big[p_{mt+1}(c^*_{it+1} + h^*_{mt+2})\Big] \\ - \beta\,\mathbb{E}_t\Big[\,\Big[\,\tfrac{1}{2}\delta h^*_{mt+1} + \boldsymbol{x_{it+1}}\gamma_x + \varepsilon_{it+1}\Big]\,h^*_{mt+1}\,\Big]\end{aligned}$$

From the law of motion, it holds that $c^*_{it+1} + h^*_{mt+2} = (1+\phi)h^*_{mt+1}$. And from the intensive margin Euler equation specified in 12, the following also holds:

$$\mathbb{E}_t\left[\tfrac{1}{2}\delta h^*_{mt+1} + \boldsymbol{x_{it+1}}\gamma_x + \varepsilon_{it+1}\right] = -\frac{1}{\beta}\alpha_p p_{mt} + \alpha_p(1+\phi)\,\mathbb{E}_t[p_{mt+1}] - \mathbb{E}_t\left[\tfrac{1}{2}\delta h^*_{mt+1}\right]$$

Therefore, I can rewrite the equation as:

$$\begin{aligned}\log\left(\frac{\rho_{mt}}{1-\rho_{mt}}\right) + \beta\gamma = &-\Psi(\boldsymbol{s_{mt}}) + \xi_{mt} - \alpha_b b_m - \xi_{mt} \\ &- \beta\,\mathbb{E}_t\Big[-\Psi(\boldsymbol{s_{mt+1}}) + \xi_{mt+1} - \log(\rho_{mt+1})\Big] \\ &- \alpha_p p_{mt} h^*_{mt+1} + \beta\alpha_p(1+\phi)\,\mathbb{E}_t\Big[p_{mt+1}h^*_{mt+1}\Big] \\ &- \beta\,\mathbb{E}_t\left[\left[-\tfrac{1}{\beta}\alpha_p p_{mt} + \alpha_p(1+\phi)p_{mt+1} - \tfrac{1}{2}\delta h^*_{mt+1}\right]h^*_{mt+1}\right]\end{aligned}$$

Which can be easily simplified and rearranged to:

$$\begin{aligned}\log\left(\frac{\rho_{mt}}{1-\rho_{mt}}\right) + \beta\gamma = &-\Psi(\boldsymbol{s_{mt}}) - \alpha_b b_m \\ &+ \beta\,\mathbb{E}_t\Big[\Psi(\boldsymbol{s_{mt+1}})\Big] - \beta\,\mathbb{E}_t\Big[\xi_{mt+1}\Big] \\ &+ \beta\,\mathbb{E}_t\Big[\log(\rho_{mt+1})\Big] + \frac{\beta}{2}\delta(h^*_{mt+1})^2\end{aligned}$$

I rearrange the previous equation and employ rational expectations, allowing me write expected values as the sum of realizations and an expectation error, to yield the equation in 4.

C.3 Instruments

C.3.1 Prices

To address the potential endogeneity of cattle prices in my regression, I employ a Shift-Share Instrumental Variable (SSIV) approach based on exogenous shocks to Chinese meat imports. This method leverages the substantial and well-documented increase in China's demand for agricultural products over the past decades, particularly since its accession to the World Trade Organization (WTO) in 2001. The instrument is constructed following the methodology of Carreira et al. (2024), which itself is theoretically grounded in the framework of Borusyak et al. (2022). This approach isolates exogenous variation in local outcomes by combining national-level shocks with initial shares of production at the regional level.

The first step in constructing the instrument involves estimating the exogenous shock component of Chinese import growth. Using detailed product-country-year trade data, I estimate an auxiliary regression to identify China-specific import growth rates for each product category[9] j. This regression excludes Brazilian data to ensure that the shocks are not influenced by domestic

[9] A product is identified by its 6-digit code in the World Customs Organization's (WCO) "Harmonized System" classification. The data used here pertains to fresh, chilled, or frozen meat from bovine animals (HS Chapter 02, Headings 01 and 02).

factors. The regression takes the following form:

$$G_{cj,t} = \gamma_{j,t} + \psi_{\text{China},\, j,t} + \epsilon_{cj,t}$$

Here, $G_{cj,t}$ denotes the growth rate of country c's imports of product j in year t, measured relative to a base year. The term $\gamma_{j,t}$ captures year-product fixed effects, varying across both products and years, to account for time-specific characteristics of each product that are invariant across countries. And $\psi_{\text{China},\, j,t}$ represents China-product-specific dummies, which isolate the component of import growth uniquely attributable to Chinese demand for product j in year t. The residual term $\epsilon_{cj,t}$ reflects any unexplained variation. I set the base year to 2000, just prior to China's World Trade Organization (WTO) accession in 2001, following Carreira et al. (2024), to ensure that the base period accurately reflects pre-treatment conditions, unaffected by subsequent policy changes.

After obtaining the estimated China-specific import growth rates ($\widehat{\psi}_{\text{China},\, j,t}$), I construct the Shift-Share Instrument as:

$$\widehat{x}_{m,t} = \sum_{j} S_{mj,\bar{t}} \cdot x_{j,\bar{t}} \cdot \widehat{\psi}_{\text{China},\, j,t} \tag{19}$$

In this expression, $S_{m,\bar{t}}$ represents the share of production in municipality m in the base year $\bar{t}$. This share is derived from the 1995 agricultural census, ensuring it predates the base year and is unaffected by subsequent shocks. $x_{j,\bar{t}}$ is the volume of Brazilian exports of product j to China in the base year. Lastly, $\widehat{\psi}_{\text{China},\, j,t}$ denotes the predicted China-specific import growth rates for product j in year t, as estimated in the auxiliary regression.

This Shift-Share variable combines the exogenous national-level shocks $\widehat{\psi}_{\text{China},\, j,t}$ with initial regional production shares $S_{m,\bar{t}}$, ensuring that the instrument captures variation in regional outcomes that stems from China's demand growth rather than from endogenous local factors. The base year values for shares and exports ensure that the comparison baseline for the shocks is pre-determined and independent of the key policy changes that triggered the shock. The use of this instrument is particularly strong for the analysis of cattle prices because Chinese meat imports have been a major driver of global demand shifts, particularly for beef. By isolating the exogenous component of this demand, the Shift-Share instrument acts as a demand shifter (Angrist et al. 2001), providing a credible strategy to address the endogeneity of prices on the supply side.

C.3.2 Pasture Quality

To address the potential endogeneity in pasture quality, I use the Palmer Drought Severity Index (PDSI) from the previous year as an instrument. Specifically, I take the lowest monthly observation within the year to capture the driest conditions experienced, which have the greatest impact on pasture quality.

The PDSI is a widely used metric for measuring drought severity by comparing current moisture levels to historical averages. I rely on monthly PDSI values calculated by Abatzoglou et al. (2018) in the TerraClimate dataset. These values are derived from a modified Thornthwaite-

Mather climatic water-balance model, which incorporates precipitation (moisture supply), reference evapotranspiration (moisture demand), and soil water storage. The reference evapotranspiration is estimated using the FAO's Penman-Monteith energy balance approach, which accounts for air temperature, solar radiation, air humidity, and wind speed.

The PDSI is a strong instrument for pasture quality because it measures soil moisture availability – a critical factor for vegetation growth and forage production. By reflecting the effects of climatic variability, the PDSI captures how droughts influence vegetation health and productivity. Its standardized design also allows for consistent comparisons of climatic stress on pasture quality across municipalities, regions, biomes, and time.

The use of minimum PDSI values focuses on the most severe drought conditions, such as the driest months or the most intense dry spells. These extreme events are particularly important for pasture quality, as they represent periods when vegetation is most stressed and forage availability is at its lowest. Using lagged values ensures the instrument's exogeneity, as past climatic conditions are predetermined and not influenced by current agricultural decisions or land-use changes.

The key assumption is that drought conditions, as measured by the PDSI, influence herd management and land-use decisions only indirectly through their effect on pasture quality. For example, severe droughts can lead to reduced forage availability, prompting farmers to adjust herd sizes (Skidmore 2023) or clear additional land for grazing (Desbureaux et al. 2018). This indirect relationship supports the validity of the PDSI as an instrument for addressing the endogeneity of pasture quality in the regression framework.

D Exercícios empíricos alternativos

D.1 Intensive margin: first stage results

Table 6: Intensive margin first stage results

Dependent Variables:	p_{mt}	p_{mt+1}	Pasture Quality (x_{mt+1})
Variables			
$ssiv_{mt}$	-19.93***	-21.23***	0.0140***
	(3.417)	(3.645)	(0.0021)
$ssiv_{mt+1}$	13.23***	14.08***	-0.0092***
	(2.261)	(2.411)	(0.0014)
pdsi_min	0.1117***	0.1100***	5.68×10^{-5}***
	(0.0201)	(0.0207)	(1×10^{-5})
Year	79.05***	59.88***	0.0075***
	(0.9454)	(0.9916)	(0.0003)
Temperature	✓	✓	✓
Past. Suit.	✓	✓	✓
Mkt. Acc.	✓	✓	✓
Transp. Cost	✓	✓	✓
Fixed-effects			
Biome	✓	✓	✓
Fit statistics			
Observations	6,487	6,487	6,487
F-test	309.45	173.59	98.484
F-test (1st stage)	49.981	47.741	38.057

Clustered (Municipality) standard-errors in parentheses
*Signif. Codes: ***: 0.01, **: 0.05, *: 0.1*

D.2 Intensive margin with municipality fixed effects

Table 7: Intensive margin FE regression results

Dependent Variable:	h_{mt+1}	
	OLS	IV
Variables		
p_{mt}	-0.0004***	-0.0004***
	(6.4×10^{-5})	(0.0002)
p_{mt+1}	0.0004***	0.0004**
	(6.18×10^{-5})	(0.0002)
Pasture Quality (x_{mt+1})	0.0953***	0.3666***
	(0.0155)	(0.0658)
Year	0.0047***	0.0069***
	(0.0014)	(0.0024)
Temperature	✓	✓
Past. Suit.		
Mkt. Acc.	✓	✓
Transp. Cost		
Fixed-effects		
Municipality	✓	✓
Fit statistics		
Observations	6,487	6,487
F-test	5,689.8	7,821.2

Clustered (Municipality) standard-errors in parentheses
*Signif. Codes: ***: 0.01, **: 0.05, *: 0.1*

D.3 Extensive margin: first stage results

Table 8: Extensive margin first stage results

Dependent Variable:	Pasture Quality ($\beta x_{mt+1} - x_{mt}$)
Variables	
pdsi_min	$-5.9 \times 10^{-5***}$
	(2.07×10^{-6})
$\frac{\beta}{2}(h_{mt+1})^2$	-0.0301***
	(0.0072)
b_m	-0.0002***
	(9.17×10^{-6})
$(\beta + (\beta - 1)t)$	0.0005
	(0.0010)
Temperature	✓
Past. Suit.	✓
Mkt. Acc.	✓
Transp. Cost	✓
Fixed-effects	
Biome	✓
Fit statistics	
Observations	6,210
F-test	106.02
F-test (1st stage)	715.73

Clustered (Municipality) standard-errors in parentheses
*Signif. Codes: ***: 0.01, **: 0.05, *: 0.1*

D.4 Extensive margin exercise with survey data

Table 9: Extensive margin regression with survey data

Dependent Variable:	$\log\left(\frac{\rho_{mt}}{1-\rho_{mt}}\right) - \beta\log(\rho_{mt+1}) + \beta\gamma$	
	OLS	IV
Variables		
$\frac{\beta}{2}(h_{mt+1})^2$	0.1171***	0.3427***
	(0.0331)	(0.1006)
Pasture Quality ($\beta x_{mt+1} - x_{mt}$)	1.382***	10.76***
	(0.0860)	(0.8078)
b_m	-0.0004***	0.0013***
	(6.79×10^{-5})	(0.0002)
$(\beta + (\beta - 1)t)$	-0.0424***	-0.0660***
	(0.0047)	(0.0054)
Temperature	✓	✓
Past. Suit.	✓	✓
Mkt. Acc.	✓	✓
Transp. Cost.	✓	✓
Fixed-effects		
Biome	✓	✓
Fit statistics		
Observations	64,736	64,736
F-test	6.6588	6.7972

Clustered (Municipality) standard-errors in parentheses
*Signif. Codes: ***: 0.01, **: 0.05, *: 0.1*

D.5 Pasture recovery effect on abatements

Figure 5: Pasture recovery counterfactual (CO_2 Abatement)

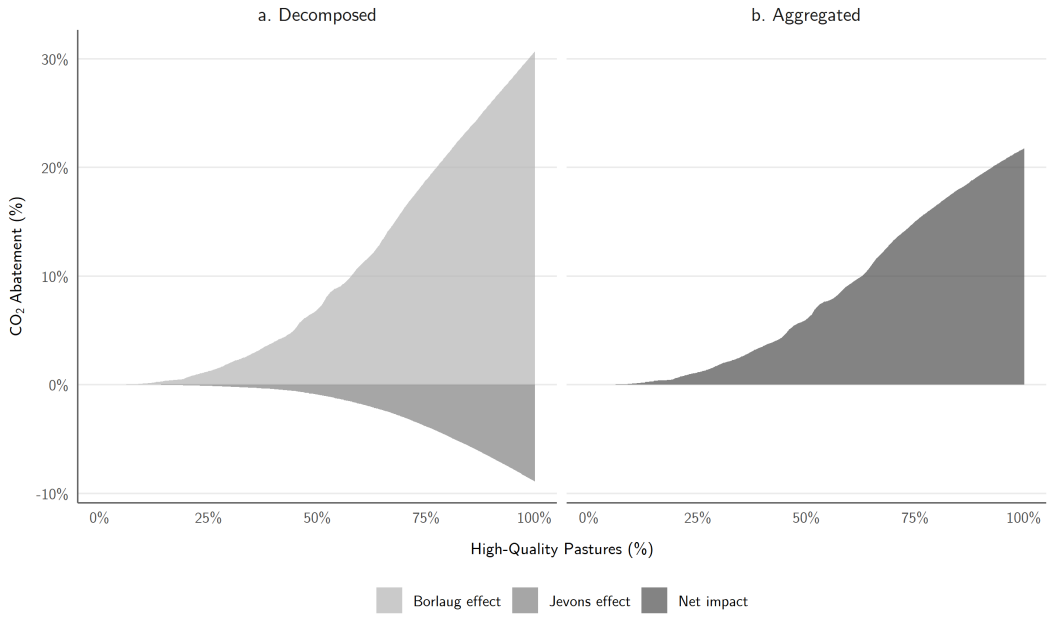

This figures plots the potential CO_2 abatement from a pasture recovery counterfactual. The X-axis shows the minimum share of high-quality pastures set by the policy in each municipality. The Y-axis shows the carbon abatement relative to the baseline emissions for each policy level. Panel **(a)** shows the disaggregation between Borlaug and Jevons effects, while panel **(b)** exhibits the net effect.